Available online at www.sciencedirect.com

ScienceDirect

Procedia Engineering 2 (2010) 2499–2504

Procedia Engineering

www.elsevier.com/locate/procedia

8th Conference of the International Sports Engineering Association (ISEA)

Multi-objective exploration of the launch condition for a fluctuating punted kick in rugby on the basis of PSP measurement

Kazuya Seo[a]*, Daisuke Yorita[b], Koji Shimoyama[c], Hiroki Nagai[b], Keisuke Asai[b]

[a]*Faculty of Education, Art & Science, Yamagata University, 1-4-12 Kojirakawa, Yamagata 990-8560, Japan*
[b]*Department of Aerospace Engineering, Tohoku University, 6-6-01 Aramaki-Aza-Aoba, Aoba-ku, Sendai 980-8579, Japan*
[c]*Institute of Fluid Science, Tohoku University, 2-1-1 Katahira, Aoba-ku, Sendai 980-8577, Japan*

Received 31 January 2010; revised 7 March 2010; accepted 21 March 2010

Abstract

We succeeded in obtaining PSP (Pressure-Sensitive Paint) measurements for a rugby ball. It was found that the seam of the ball is the trigger for initiating low pressure. Therefore, a slower spinning ball fluctuates during flight because of the asymmetrical pressure distribution on the sides of the ball. Based on the results from PSP measurements, multi-objective optimization of the fluctuating punted kick was carried out, and then the trade-offs between the objective functions and the control variables could be visualized using Self-Organizing Maps. It was found that the higher the spin rate at launch the greater the number of fluctuations; however, the hang time becomes shorter.

Keywords: rugby; pressure-sensitive paint; multi-optimization; data mining; fluctuating punted kick

1. Introduction

Ideally, in a rugby game, a punted kick is caught by the team kicking the ball, since the team retains possession. However, it is often difficult for a team representing Japan to catch a punted kick because of the generally shorter height of the Japanese players compared to representative teams from other countries. Therefore, it is desirable to make catching difficult for the taller opposition. One of the techniques to cause such difficulty is a fluctuating punted kick, and this type of kick is the subject of this study. In a previous study [1], we found that the side force acting on a rugby ball depends on the position of the seam as well as the angle of attack. There is a possibility of the side force being either positive or negative depending on the position of the seam and the angle of attack. Simulation of the ball flight trajectory showed that a punted kick rotating at low spin rates fluctuates during flight.

In this paper, a PSP (Pressure-Sensitive Paint) measurement was carried out on a scaled model to measure the pressure distribution on the surface. It is difficult to apply PSP to low-speed flow. The dynamic pressure at 50m/s

* Corresponding author. Tel.: +81-23-628-4350; fax: +81-23-628-4454.
E-mail address: seo@e.yamagata-u.ac.jp.

1877-7058
doi:10.1016/j.proeng.2010.04.022

(1.5 kPa) is comparable to the measurement accuracy of the PSP measurement. Recently, however, there has been a breakthrough in the PSP measurement technique for low-speed flow [2]. The key is to reduce measurement errors, such as optical noise, model displacement, and temperature distribution over the model. We succeeded in obtaining PSP measurements for a rugby ball in the same manner. Moreover, an optimization of the fluctuating punted kick is carried out using a genetic algorithm [3]. It was assumed that there are five objective functions and nine control variables in this case. The nine control variables, which are under the control of the kicker, determine the launch conditions. Since the control variables are too many to enable the optimal values to be determined manually, the optimization study is clearly necessary in order to find the optimal punted kick. Since the present optimization problem considers multiple objective functions, it has not a unique but multiple optimal solutions, which are the so-called Pareto-optimal solutions named after the Italian economist. Four of the five objective functions are concerned with the ball fluctuations in the forward and lateral directions, whereas the fifth is the hang time. A long hang time reduces the chances of the opposition being able to mount a counter-attack by tackling them immediately after the catch. Finally, for the Pareto-optimal solutions, the trade-offs between the objective functions and the control variables are visualized. Generally, it is not possible to visualize the relationship among the variables simply by plotting the solutions when there are more than three variables, as in the present study with 14 variables (5 objective functions + 9 control variables). By using Self-Organizing Maps (SOMs [4]) as a data mining tool for the visualization of the relationship in the many-variable space, it is possible to obtain the entire trade-off features in a comprehensive manner [5]. The value itself is not so important, but the trade-off features or entire trend should be known by player and coaches.

2. Methods

2.1. PSP measurements

PSP consists of luminescent molecules, a polymer binder and a solvent. The mechanism of PSP measurement is based on oxygen quenching. The luminescence increases if the amount of oxygen decreases, while the amount of oxygen decreases if the pressure is low. Therefore, the lower the pressure, the brighter the luminescence.

A wind speed of 50m/s was applied in this experiment. A 30 % scaled model of a rugby ball was employed so that the Reynolds number would be in a practical range. The model was made of aluminum in order to prevent a temperature gradient forming in it. There were four channels on the surface representing the seams on the surface of a ball. PSP was sprayed to the model. Two semi-ellipsoids made of aluminum were joined together by screws. A Front view of the experimental set-up is shown in Fig. 1. There is an oval shape which is clay that has been used to fill up the hole used for the screw. The electrical wires along the strut are connected to a thermocouple for temperature measurement, and the tubes are connected to a pressure transducer in a port of 0.3 mm diameter for static pressure measurement. In the PSP, the luminescent molecule is PtTFPP[6], the polymer binder is FIB[7], and the solvent is benzene. The schematic of the optical system is shown in Fig. 2. Two UV-LED units and a 16-bit cooled CCD camera (HAMAMATSU, C4742-98) were used. Band filters were placed in front of both the LEDs and the camera to cut the parasitic emission and absorption.

Fig. 1. Front view of the scaled model

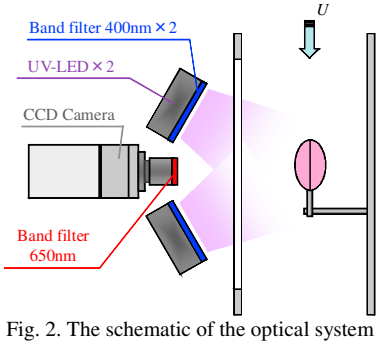

Fig. 2. The schematic of the optical system

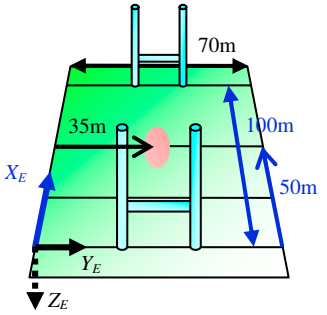

Fig. 3. Inertial coordinate system

2.2. Multi-objective exploration

Multi-objective exploration is composed of two parts. One is the multi-objective optimization by using an elitist genetic algorithm, and the other is the data mining by using SOM. The punted kick from the center of the field is optimized. The initial ball position is assumed to be (X_E, Y_E, Z_E) = (50, 35, -0.5) as shown in Fig. 3. The X_E-axis is along the left hand touch line, the Y_E-axis along the kicker's goal line with the origin at the intersection of these. The Z_E-axis is vertically downward.

The nine control variables are shown in Table 1. The ranges of these, also shown in Table 1, are defined such that they cover practical values. Six of the nine control variables are concerned with the velocity vector (Fig. 4) and the angular velocity vector, and the other three are concerned with the Eulerian angles. The Eulerian angles represent the attitude of the ball with respect to the inertial coordinate system. If the nine control variables are given, the flight trajectory is obtained.

Table 1. Control variable

Control variables	Abb.	Ranges
cv1= Magnitude of the velocity vector	V_0	$15 < V_0 < 25$ m/s
cv2= Elevation angle of the velocity vector	γ_0	$15 < \gamma_0 < 85$ °
cv3= Azimuth angle of the velocity vector	χ_0	$-90 < \chi_0 < 90$ °
cv4= Magnitude of the angular velocity vector	ω_0	$0<\omega_0<1$ rev./sec.
cv5= Elevation angle of the angular velocity vector	ι_0	$-90 < \iota_0 < 90$ °
cv6= Azimuth angle of the angular velocity vector	κ_0	$-90 < \kappa_0 < 90$ °
cv7= Yaw angle	Ψ_0	$-90 < \Psi_0 < 90$ °
cv8= Pitch angle	Θ_0	$-90 < \Theta_0 < 90$ °
cv9= Roll angle	Φ_0	$0 < \Phi_0 < 360$ °

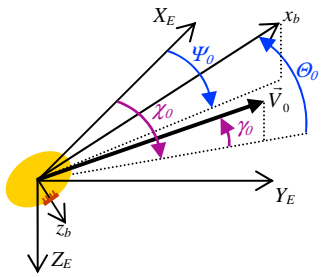

Fig. 4. velocity vector

Table 2. Objective function

Objective function	Physical meaning
F1= number of direction change in the X_E-axis	The number of fluctuation in the X_E-axis during the flight. Maximize F1 (higher # of fluctuation in the X_E-axis is better.).
F2= number of direction change in the Y_E-axis	The number of fluctuation in the Y_E-axis during the flight. Maximize F2 (higher # of fluctuation in the Y_E-axis is better.).
F3= Σt_i	Summation of t_i (t_i : time at the instance when the direction changes in the X_E-axis.) Maximize F3 (higher # of fluctuation in the X_E-axis at the very last time is better.).
F4= Σt_j	Summation of t_j (t_j : time at the instance when the direction changes in the Y_E-axis.) Maximize F4 (higher # of fluctuation in the Y_E-axis at the very last time is better.).
F5= t_f	The hang time t_f Maximize F5 (longer hang time is better.).

Five objective functions, *F1, F2, F3, F4* and *F5* as shown in Table 2 are considered. The hang time is denoted by *F5*, and the other four, *F1* to *F4*, are concerned with the fluctuation of the flight trajectory. *F1* denotes the total number of changes in the X_E direction during flight, and *F2* denotes that in the Y_E direction. On the other hand, the timing of the fluctuations is considered in *F3* and *F4*. t_i and t_j denote the time at the instance when the direction changes in the X_E and Y_E direction, respectively. It seems that fluctuations in the falling phase of the punted kick makes the catch more difficult when compared with fluctuations in the rising phase. The later in its flight the ball fluctuates, the larger the values of *F3* and *F4* (Σt_j and Σt_j), which indicates the most desirable situation. It might be intuitively considered that *F3* is equivalent to *F1*, and *F4* is equivalent to *F2*. However, the present study

distinguishes those functions without such intuition. All the objective functions can be estimated by obtaining the flight trajectory.

The following constraints are imposed: $t_f \geqq 1$[sec.]---(1), $65 \leqq X_E(t_f) \leqq 90$[m]---(2), $0 \leqq Y_E(t_f) \leqq 70$[m]---(3), $\omega(t) \leqq 1$[rev./sec.]---(4). The first constraint (1) means that the hang time should be at least 1 second, and the second constraint (2) that the flight distance in the forward direction is more than 15 meters and less than 40 meters for a practical punted kick. Constraint (3) signifies that the ball should make contact with the ground within the field-of-play. Constraint (4) means that the magnitude of the angular velocity vector should be less than 1 revolution per second during the whole flight. It is assumed that, at a slow spin rate less than 1 rev./sec., the ball is in a quasi-steady state. In this optimization, all the objective functions must be maximized. An elitist multi-objective genetic algorithm was applied for the optimization. The procedure is outlined in Ref [8].

The visualization between all the variables is accomplished by using a SOM so that the whole trend can be visualized. A SOM is a type of artificial neural network that trains a set of high-dimensional input data through an unsupervised learning process, and projects them onto a low-dimensional output map while preserving their own features. In this study, SOMs were generated in the hexagonal topology by using Viscovery® SOMine 5.0 (MindWare,Inc.).

3. Results

3.1. PSP measurements

The results of the PSP measurement are shown in Fig.5. These show contour maps of the pressure coefficient, C_P. White denotes the highest value of 1.0, while black denotes the lowest value of -2.5. The small black dots on each figure are markers to calibrate the position, and the relatively large black oval in Fig. 5-(d) is the clay filling. The seam angle dependence is shown in Fig. 5 as well as the result on an ellipsoid (Fig. 5-(a)). The seam angle, σ, denotes the position of the seam. With the longitudinal axis perpendicular to the wind direction, the seam angle σ is defined as 0° if the seam is situated facing the wind, equals 30° when it rotates 30° on its longitudinal axis.

It can be seen that the low pressure appearing at σ = 60° doesn't appear at σ = 0 or 30° or on the ellipsoid. In other words, the seam at σ = 60° is the trigger for initiating the low pressure, whereas, with the seam at σ = 0 or 30°, it doesn't act as a trigger. It seems that the seam at σ = 30° is too close to the stagnation point so that it doesn't trigger turbulence because of the low wind speed at the seam at σ = 30°. These results consist with the seam angle dependence on the side force [1]. It was confirmed that a punted kick rotating at low spin rates fluctuates from side to side during the flight.

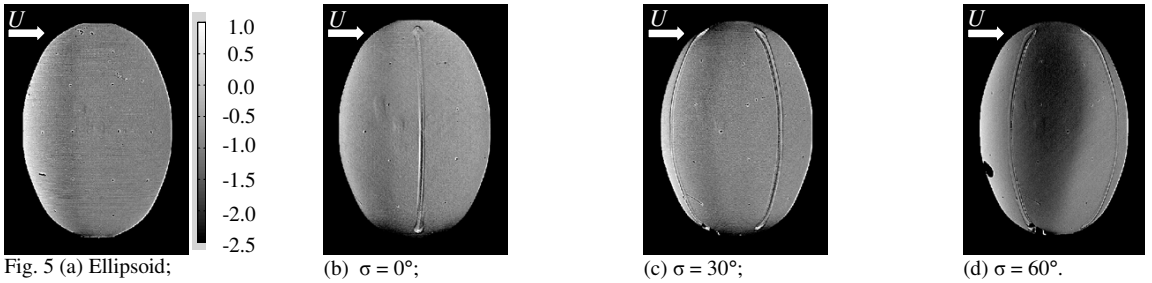

Fig. 5 (a) Ellipsoid; (b) σ = 0°; (c) σ = 30°; (d) σ = 60°.

Fig. 5. Pressure distribution.

3.2. Multi-objective exploration

Although the highest value is ideal for each of the objective functions, it is impossible for all the objective functions to become highest simultaneously. It is because the objective functions conflict with one another. Therefore, multi-objective optimization involves a set of the solutions, each of which is better regarding one objective function but worse regarding the others. These kinds of objective-conflicting solutions are called "Pareto-optimal solutions," and represent the trade-off features among the objective functions. Fig. 6 shows the flight

trajectory in the case of the longest hang time. It fluctuates during flight. This solution corresponds to the solution that is optimized regarding a single objective (hang time) but not optimized regarding the other objectives. This kind of solution is called an extreme optimal solution. The maximum height is more than 30 meters for which the longest hang time of 5.45 sec. is attained. Although the maximum value for the hang time has been found, other Pareto optimal solutions have not been examined. The questions are what the entire trend is, and which control parameters are essential for each objective function.

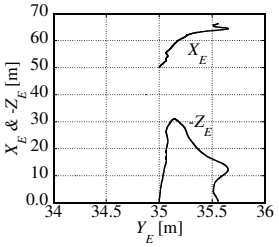

Fig. 6. The flight trajectory in the case of the longest hang time.

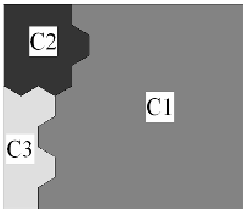

Fig. 7. Cluster.

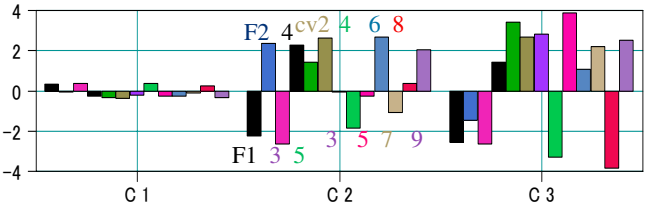

Fig. 8. Features of clusters.

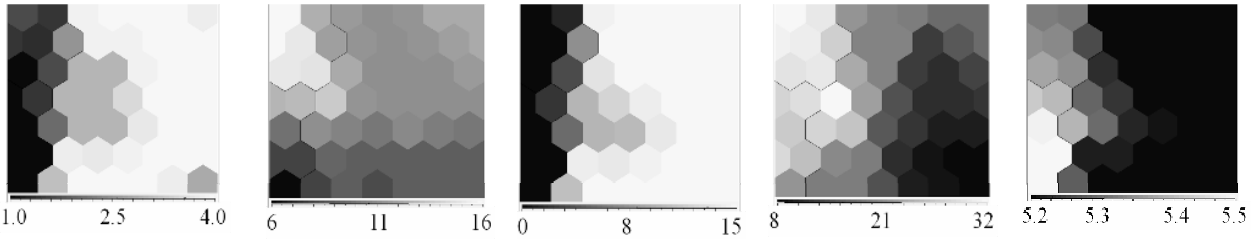

Fig. 9 (a) F1; (b) F2; (c) F3; (d) F4; (e) F5.
Fig. 9. Self-organizing maps for objective functions.

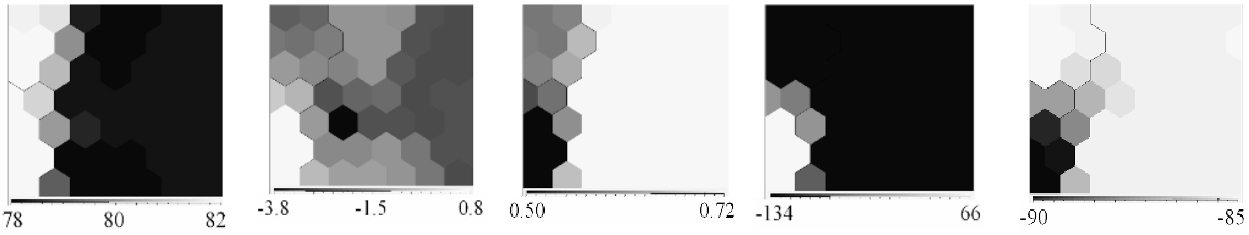

Fig. 10 (a) cv2; (b) cv3; (c) cv4; (d) cv5; (e) cv8.
Fig. 10. Self-organizing maps for control variables.

Fig.7 shows three clusters on the basis of the SOM-Ward method. 88% of Pareto-optimal solutions belongs to cluster 1(*C1*), while 6%, each, belongs to *C2* and *C3*. Fig.8 shows the features of the clusters. The ordinate denotes the deviation from each average value. There are thirteen bar graphs for each cluster. Five of thirteen are objective functions, *F1* to *F5*, while the other eight are control variables, *cv2* to *cv9*. Since *cv1* (magnitude of the velocity vector) is almost 25m/s for all Pareto-optimal solutions, it is not shown. In *C1*, all objective functions and control variables are close to the average value, although *F1* & *F3* are relatively large and *F4* & *F5* are small. In *C2*, however, *F2* & *F4* are the largest. This means that the punted kick in *C2* fluctuates more in the Y_E-axis. In *C3*, *F5* becomes the largest, while *F1*, *F2* & *F3* becomes smaller. Therefore, the hang time in *C3* is the longest. SOMs of the objective functions are shown in Fig. 9. These are the contour maps colored by each objective function value. The black denotes the lowest value, while the white denotes the highest. It can be seen that *C3* in Fig.7 corresponds to the largest *F5* (Fig.9-(e)) and the smaller *F1, F2* & *F3* (Fig.9-(a), (b) & (c)), as shown in Fig.8. *C2* in Fig.7 corresponds to the intermediate case of *F5* in Fig.9-(e) and the largest case of *F2* & *F4* (Fig.9-(b) & (d)). In *C1*, *F4* & *F5* are relatively small and *F1* & *F3* are large. The highest number of fluctuations in the Y_E direction is sixteen for the Pareto-optimal solutions, while the lowest number is six as shown in Fig.9-(b). It can be seen from Figs.9-(b)

and 9-(d) that the color patterns of the contour maps are almost same. The pattern matching can be seen between Figs.9-(a) and 9-(c), too. Therefore, it can be concluded that the total number of fluctuations in the X_E and Y_E directions (*F1* & *F2*) are almost equivalent to the objective functions (*F3* & *F4*) in which the timing of the fluctuations is considered. The contour maps of Figs.9-(a) and 9-(c) are almost the converse of that in Fig.9-(e). The extreme case of the longest hang time, shown in Fig.6, is located at the bottom left hand side of the SOM, where *F5*(Fig.9-(e)) shows the highest value of the hanging time and *F1*, *F2* & *F3* (Fig.9-(a) to 9-(c)) show almost lowest values. This means that there is a trade-off between *F5* and *F1*, *F2* & *F3*.

SOMs for a typical five of eight control variables are shown in Fig. 10. A contour map, similar to *F5* (Fig. 9-(e)), can be seen for *cv2* (Fig.10-(a)), *cv3* (Fig.10-(b)) and *cv5* (Fig.10-(d)). A contour map, the converse of *F5,* can be seen for *cv4* (Fig.10-(c)) and *cv8* (Fig.10-(e)). This means that the hang time is influenced by these control variables. It can be seen from Fig.9-(a) to 9-(c) and Fig.10-(c) that the higher the spin rate the larger the number of fluctuations. This is because a higher spin rate changes the seam angle and the angle of attack more frequently, thus changing the sign of the side force more frequently. The amplitude of the fluctuations becomes smaller because of the frequent sign change. As shown in the trade-off between the hang time and the other objective functions, the hang time becomes shorter when the spin rate is higher. This is because the frequent variations in the projected area reduce the maximum height. The opposite situation happens in the case of a lower spin rate. It can also seen from Figs.9-(e) and 10-(a) that a larger *cv2* (flight path angle) makes *F5* (flight time) longer. Close to 90°, *cv2* increases the maximum height. When *cv3* (azimuth angle of the velocity vector, Fig.10-(b)) is not close to 0°, the number of fluctuations in the X_E direction (Fig.9-(a)) increases. Deviation from an azimuth angle of 0° means that the flight trajectory slants into touch rather than towards the goal line. *cv3* (Fig.10-(b)) contributes to fluctuations in the X_E direction (Fig.9-(a)) by changing the sign of the side force. From Figs.10-(e) and 9-(e), a pitch angle, *cv8*, of -90° corresponds with the longest hang time. The angle of -90° is the situation in which the longitudinal axis lies in the vertical direction. The initial pitch angle of -90° renders the drag small in the rising phase so that the maximum height has a high value, and the flight time becomes long.

4. Conclusion

We succeeded in obtaining PSP measurements for a rugby ball, and carried out multi-objective exploration of the launch condition for a fluctuating punted kick. The results can be summarized as follows.

1) From PSP measurements, the seam of the rugby ball was the trigger for initiating low pressure.

2) The trade-off features or entire trend in the many-variable space could be visualized by using SOMs.

3) There is a trade-off between the hang time and the number of fluctuations.

4) The higher the spin rate at launch the greater the number of fluctuations; however, the hang time becomes shorter.

References

[1] Seo K., Kobayashi O. & Murakami M. Regular and irregular motion of a rugby football during flight. *The Eng. of Sport 5* 2004, **1:** 567–573.

[2] Yamashita T., Sugiura H., Nagai H., Asai K. and Ishida K. Pressure-Sensitive Paint Measurement of the Flow around a Simplified Car Model. *Journal of Visualization* 2007, **10**: 289–298.

[3] Deb, K. *Multi-Objective Optimization using Evolutionary Algorithms.* New York: Wiley; 2002.

[4] Kohonen T. Self-Organizing Maps, Berlin, Heidelberg: Springer; 1995.

[5] Obayashi S. and Sasaki D. Visualization and Data Mining of Pareto Solutions Using Self-Organizing Map. Evolutionary Multi-Criterion Optimization, *Lecture Notes in Computer Science*, Springer-Verlag; 2003, 796-803.

[6] Bell, J.H., Schairer E.T., Hand L.A. and Mehta R.D. Surface pressure measurements using luminescent coatings, *Annu Rev Fluid Mech* 2001; **33**: 155.

[7] Puklin E., Carlson B., Gouin S., Costin C., Green E., Ponomerev S., Tanji H. and Gouterman M. Ideality of pressure-sensitive paint. I. Platinum tetra (pentafluoropheny) porphine in fluoroacrylic polymer, *J Appl Polymer Sc.* 2000; **77**: 2795-2804.

[8] Seo K., Kobayashi O. and Murakami M. Multi-optimization of the screw kick in rugby by using genetic algorithm. *Sports Engineering* 2006, **9**: 87-96.